arXiv:astro-ph/0107491v1 25 Jul 2001

Globular Cluster Population of Hickson Compact Group 22a and 90c[1]

Wayne A. Barkhouse

Department of Astronomy & Astrophysics, University of Toronto, Toronto, Ontario, Canada, M5S 3H8

barkhous@astro.utoronto.ca

Michael J. West

Department of Physics & Astronomy, University of Hawaii at Hilo, Hilo, HI 96720

west@bohr.uhh.hawaii.edu

and

Gregory D. Bothun

University of Oregon, Department of Physics, Eugene, OR, USA, 97403

nuts@moo.uoregon.edu

ABSTRACT

We present the first measurement of the globular cluster populations of galaxies in Hickson compact groups, in order to investigate the effect of these high density environments on the formation and evolution of globular cluster systems. Based on V and R band images that we obtained of HCG 22a and HCG 90c with the ESO New Technology Telescope (NTT), we find a total globular cluster population of 1590 ± 854 for HCG 22a and 2136 ± 718 for 90c. The specific frequency for HCG 22a was found to be $S_N = 1.9 \pm 1.0$ and $S_N = 3.4 \pm 1.1$ for HCG 90c. A power-law fit to the globular cluster radial profile of HCG 22a yields $\sigma \sim R^{-2.01\pm0.30}$ and for HCG 90c we found $\sigma \sim R^{-1.20\pm0.16}$. A comparison of the globular cluster radial profiles with the surface brightness of the parent galaxy shows that the globular cluster systems are at least as extended as the halo light. The measured values for the specific frequency are consistent with a scenario in which the host galaxies were in a low density "field-like" environment when they formed their globular cluster systems.

Subject headings: galaxies: compact groups—galaxies: individual (NGC 1199, NGC 7173)—globular clusters: general

1. Introduction

Tremendous progress has been made in recent years in the detection of globular cluster (GC) populations around galaxies beyond the Local Group (e.g., Harris 1991; Blakeslee 1999). The globular cluster populations of well over 100 galaxies up to distances $\gtrsim 100h^{-1}$ Mpc have now been studied in various environments in the hope of gaining further insight into galaxy formation and evolution. Studies have shown that the number of globular clusters associated with any particular galaxy varies widely, from none for M32 to $\sim 20,000$ for the cD galaxy M87 (e.g., Harris 1991).

A useful parameter for quantifying the total number of globular clusters per galaxy is the specific frequency, $S_N = N_{tot}10^{0.4(M_V+15)}$, which is

[1]Based on observations collected at the European Southern Observatory, Chile.

defined as the total number of globular clusters, N_{tot}, per unit galaxy luminosity (normalized to $M_V = -15$; Harris & van den Bergh 1981). Previous studies have shown that globular cluster populations vary systematically with galaxy type and environment (Harris 1991; West 1994). Characteristic values of S_N range from $S_N \leq 1$ for field spiral galaxies, to $S_N \simeq 2-4$ for field ellipticals, to $S_N \simeq 5-7$ for ellipticals in dense environments, and up to $S_N \simeq 10-20$ for supergiant ellipticals at the centers of rich clusters. (We note that normalization with respect to bulge luminosity for spiral galaxies would increase the value of S_N, see Côte et al. 2000.) Yet, which factor has the greatest influence on globular cluster formation—galaxy type or environment—is unclear.

Several competing theories have been proposed to explain the origin of the observed variations in globular cluster systems of different galaxies. Among these are: galaxy mergers (Schweizer 1986; Ashman & Zepf 1992), accretion via tidal stripping or merging (Côte, Marzke, & West 1998; Côte et al. 2000), and two-stage collapse models (Forbes, Brodie, & Grillmair 1997). At present, it is unclear whether a single mechanism, or a combination of proposed formation scenarios, can explain the properties of globular cluster systems (Kissler-Patig 2000). Determining which scenario most accurately describes the formation of globular clusters will require the investigation of GC systems in a wide range of environments.

In this paper we present observations of the globular cluster population of two galaxies in Hickson compact groups; HCG 22a (NGC 1199) and HCG 90c (NGC 7173). Compact groups are interesting because, although they are small (typically 3–7 member galaxies per group), they are extremely dense systems, comparable in density to the cores of rich Abell clusters (e.g., Hickson 1982; Hickson et al. 1992). This makes them a useful tool for probing the influence of environment on globular cluster formation.

Figure 1 and 2 show V band images of HCG 22a and 90c, respectively. Both HCG 22 and 90 have been detected by ROSAT and each group has been shown to be a weak X-ray source (Ponman et al. 1996). Table 1 summarizes the general properties of these systems. We discuss each in detail below.

1.1. Hickson Compact Group 22

HCG 22 initially was thought to contain five members (three ellipticals and two spirals) but later redshift measurements determined that two of the elliptical galaxies (HCG 22d and 22e) were most likely background galaxies since their heliocentric radial velocities are ~ 7000 km s^{-1} greater than the remaining group members (Hickson et al. 1992). The median heliocentric radial velocity of the three bona fide group members is 2700 km s^{-1}, with a velocity dispersion of 43.7 km s^{-1}.

From Table 1, the heliocentric velocity of HCG 22a is 2705 km s^{-1} which indicates that this galaxy is most likely located near the group center of mass. Hickson et al. (1992) estimated the mass-to-light ratio of HCG 22 to be $M/L \sim 1.3h^{-1}M_{\odot}/L_{\odot}$ and a projected median galaxy-to-galaxy separation of $26.9h^{-1}$kpc. The group crossing time, defined as the ratio of the crossing time to the age of the universe, is $Ht_c = 0.1905$ which is greater than the median value of $Ht_c = 0.016$ determined for all of the Hickson compact groups combined (Hickson et al. 1992). This suggests that galaxy mergers and interactions may be less important for HCG 22 than for other compact groups with shorter crossing times.

1.2. Hickson Compact Group 90

HCG 90 consists of four bright galaxies (two ellipticals, a spiral, and an irregular) with a median heliocentric group radial velocity of ~ 2640 km s^{-1} and a velocity dispersion of ~ 100 km s^{-1} (Hickson et al. 1992). The mass-to-light ratio of HCG 90 is given by Hickson et al. (1992) as $M/L \sim 12.3h^{-1}M_{\odot}/L_{\odot}$ and a median projected galaxy separation of $29.5h^{-1}$kpc. Table 1 lists the heliocentric radial velocity of HCG 90c as 2696 km s^{-1}, which indicates that this galaxy is probably close to the center of mass of the group.

The group crossing time was estimated by Hickson et al. (1992) to be $Ht_c = 0.0224$, which is only $\sim 12\%$ of the estimated value for HCG 22. This suggests that galaxy mergers and interactions are likely to have been more important in HCG 90 than for HCG 22 and it is interesting to note that HCG 90 contains a galaxy (HCG 90d) that is clearly interacting with other group members (Longo et al. 1994; Plana et al. 1999).

In this study, we have measured the globular

cluster specific frequency of HCG 22a and HCG 90c. In § 2 we present the observations and data reductions. Section 3 presents the results for HCG 22a and 90c in terms of their globular cluster luminosity functions, radial distributions, and specific frequencies. In § 4 we discuss the results of this study in the context of globular cluster formation and the nature of Hickson compact groups.

Throughout this paper, unless otherwise specified, we use $H_0 = 50$ km s^{-1}Mpc^{-1}.

2. Observations and Data Reductions

Observations of HCG 22a and 90c were obtained on the nights of October 9 and 10, 1993 using the 3.5m New Technology Telescope (NTT) operated by the European Southern Observatory (ESO) in La Silla, Chile. All images were taken with the ESO Multi-Mode Instrument (EMMI) with a Loral 2048 CCD mounted on the red arm. The Loral 2048 CCD chip consists of 2048×2048 15μm pixels, giving a scale of $0.29''$ per pixel at the f/11 Nasmyth focus. Technical limitations during the observing run limited the effective area of the chip to 1700×1700 pixels, resulting in a projected sky coverage of $8.2' \times 8.2'$.

The observations consisted of 5×900 second exposures in the Cousins V and R passband for HCG 22a, and 6×900 seconds in V and R for HCG 90c. Since globular clusters around these galaxies can be detected only as a statistical excess of star-like objects, a series of 5×900 second exposures in V and R were also taken of a control field located within 3° of the target galaxies in order to ascertain the expected number of contaminating Galactic stars and unresolved faint galaxies along the line of sight. The seeing varied during the observing run from $0.87''$ to $0.98''$ (FWHM), as measured from the individual galaxy frames.

Processing of the raw images was conducted within the IRAF[2] environment and involved the standard procedure of bias correction and flat fielding using dome flats. After this initial processing, each set of individual galaxy and control field images were registered to their common coordinate system and median combined to yield a higher S/N image. Instrumental magnitudes were transformed to the standard UBVRI system by measuring several standard stars from Landolt (1992).

At the distance of the target galaxies ($\sim$ 54 Mpc), and with the typical seeing of the combined frames ($\sim 0.9''$), individual globular clusters are unresolved and appear as an apparent excess of star-like objects around their parent galaxy. In order to maximize the detection of individual globular clusters and to perform accurate photometry, the light from each host galaxy was removed. This was done by using the STSDAS package in IRAF to model the light distribution of each galaxy using the tasks `ellipse` and `bmodel`, which fit isophotes and then generate models of each galaxy's surface brightness profile. The constructed galaxy models were then subtracted from the appropriate image.

The galaxy-subtracted image of HCG 22a revealed a large, central, diffuse structure which is the residual of a known central dust lane (Franx, Illingworth, & Heckman 1989). In order to remove this feature, the galaxy-subtracted image was median filtered using a ring median filter (Secker 1995) having an inner radius of 6.36 pixels and a width of 1 pixel. The resultant smoothed image was subtracted from the previous image, which helped to remove most of the dust lane feature. A second rectangular median filter of dimension 10×10 pixels was applied to the resultant image and this smoothed image was subtracted from the previous image. The galaxy light removal procedure was applied equally to the V and R images.

The HCG 90c galaxy model was subtracted from the parent image and the result was median filtered using a ring filter with the same dimension as that used for HCG 22a. The resultant smoothed image was then subtracted from the previous image, adequately removing all galaxy light. This procedure was applied equally to the V and R images.

Object detection and classification was conducted using the Faint Object Classification and Analysis System (FOCAS) within the IRAF environment (Jarvis & Tyson 1981; Valdes 1993). A threshold of 2.5σ above background and a minimum object area of six pixels was used for the detection criteria. The detected objects were classified by FOCAS as star-like or galaxy-like by comparing a model PSF, generated by the average

[2]IRAF is distributed by National Optical Astronomy Observatories, which are operated by the Association of Universities for Research in Astronomy, Inc., under cooperative agreement with the National Science Foundation.

profile of a minimum of ten isolated, unsaturated stars, with the light profile of each object. The object list was then culled of saturated and galaxy-like objects. A master catalog of stellar-like objects detected in both the V and R images was generated for each galaxy and the control field. Only objects that were matched in both filters were included in the final sample, thereby greatly reducing the possibility of false detections of objects. DAOPHOT was used to perform the photometry on all detected objects.

Extinction corrections (Burstein & Heiles 1982) were determined to be negligible for HCG 90 and the control field ($A_B = 0.0$). For HCG 22, we determined $A_V = 0.08$ magnitude and $A_R = 0.06$ magnitude.

2.1. Completeness Function

Since the globular cluster population of HCG 22a and 90c are detected only at very faint magnitudes ($V \geq 22$), the probability of detecting an object as a function of magnitude must be determined as accurately as possible. A "completeness" function was calculated by adding artificial stars (generated using the DAOPHOT routine `Addstar`) to the galaxy and control field images and then re-running the FOCAS routines. The fraction of detected artificial stars as a function of magnitude was then used to derive the completeness function.

Artificial stars were added to both the V and R images using the same spatial coordinates and with $V - R = 0.4$ (the approximate color of Milky Way globular clusters; see Peterson 1993). FOCAS was then run *exactly* in the same manner as that used for real objects, including keeping only those objects detected in both the V and R images.

The photometric magnitude limit of the data is defined as the magnitude at which the probability for detecting an object equals 50% (Harris 1990) . For magnitudes fainter than this limit, object information is much less reliable and thus all such objects were discarded from further analysis. The completeness limit for HCG 22a was determined to be $V = 24.9$.

Since noise and degree of crowding increases towards the center of the subtracted galaxy, the completeness function will vary with radial distance from the galaxy center. Artificial stars were placed at different radii from the galaxy center and the completeness limit, as a function of radial distance, was measured. The completeness function was measured as a function of both magnitude and position from the center of the subtracted galaxy.

For HCG 22a, it was determined that for radii < 70 pixels, the completeness limit was several magnitudes brighter than for radii > 70 pixels (part of this is due to the small disk-like artifact found at the center of HCG 22a). All objects found within 70 pixels of the galaxy center were discarded and this inner region was not used in any further analysis. For the area outside of this region, the completeness function was found to be approximately the same.

For HCG 90c, the area within 60 pixels of the galaxy center was determined to be unusable due to its bright magnitude completeness limit. This region was masked out and not used in any further analysis. The completeness limit of the area outside of this region was determined to be $V = 24.8$.

For the control field, artificial star experiments indicate a completeness limit of $V = 24.6$.

Photometric errors were calculated by determining the standard deviation of the magnitude difference between added and recovered artificial stars. The root-mean-square of the random error for HCG 22a ranged from $\sigma_{rms} \approx 0.01$ at $V = 22$ to $\sigma_{rms} \approx 0.06$ at $V = 24.6$. For HCG 90c, $\sigma_{rms} \approx 0.01$ at $V = 22$ and increased to $\sigma_{rms} \approx 0.09$ at $V = 24.6$.

2.2. Selection Criteria

The detection of globular cluster candidates can be improved using criteria such as magnitude and shape parameters which are characteristic of globular clusters in general. Since objects detected in both galaxy fields must be compared to objects detected in the control field, all objects in the galaxy image catalogs with magnitudes fainter than $V = 24.6$ (the completeness limit of the control field) were culled. Also, at the distance of HCG 22a and 90c, the number of globular clusters brighter than $V = 22$ is negligible and hence all objects brighter than this limit were removed from the object catalogs.

Besides the magnitude criteria, all objects that lie within the masked regions (such as near the galaxy centers and regions containing bright

galaxies) were eliminated from the object catalogs. In order to improve the S/N of detected globular clusters over background galaxies, all objects detected more than $2.13'$ from the center of HCG 22a were discarded (at this radius the density of globular cluster candidates becomes negligible; see section 3.2). For HCG 90c, a cutoff radius of $2.58'$ was chosen.

Figures 3 and 4 depict the spatial distribution of globular cluster candidates for HCG 22a and HCG 90c. A concentration of star-like objects surrounding each galaxy center is clearly seen.

Figures 5, 6, and 7 give the color-magnitude distribution for the galaxy and control fields. It appears from these figures that the distribution of stellar-like objects in HCG 22a and HCG 90c are generally more concentrated at a specific color than those objects found in the control field. Due to the small number of detected objects and the very short color baseline, we have not imposed a color selection criteria.

3. Results

3.1. Globular Cluster Luminosity Function

At a limiting magnitude of $V \simeq 24.6$ we sample only the brightest fraction of globular clusters present around HCG 22a and 90c. Consequently, it is necessary to extrapolate counts to include the more numerous faint globulars not detected in our images.

Globular cluster luminosity functions are universally well described by a Gaussian function (Harris 1991) of the form

$$N(V) = A\ exp\left[\frac{-(m-m_o)^2}{2\sigma^2}\right], \qquad (1)$$

where $N(V)$ is the number of globular clusters, A is the amplitude, m is the apparent magnitude of individual globular clusters, m_o is the magnitude of the turnover, and σ is the dispersion.

The globular cluster luminosity function (GCLF) for each galaxy was constructed from the statistical subtraction of star-like objects measured from the control field. Unresolved objects in the galaxy field will consist of true globular clusters, foreground stars, and faint background galaxies which have stellar-like profiles and were miss-classified by FOCAS. In fact, most of the contamination will be due to faint unresolved galaxies since one expects less than one foreground star per square arcminute at $V > 21$ (e.g., Ratnatunga & Bahcall 1985). Since object detection and classification were carried out identically for both the galaxy and control fields, the difference in the number of star-like objects between the galaxy fields and the control field (corrected for completeness and normalized with respect to spatial coverage) should be, statistically, globular cluster candidates.

Fitting a Gaussian function to the GCLF data involves simultaneously fitting three parameters; the turnover, dispersion, and the amplitude. However, since the GCLF data for HCG 22a and 90c are highly uncertain near the completeness limit, it was decided not to attempt to simultaneously solve for all three parameters. The absolute magnitude of the turnover of the GCLF is observed to be roughly the same for all galaxies, regardless of morphological type or local environment (Harris 1991; Jacoby et al. 1992). We have therefore adopted $M_V = -7.4 \pm 0.2$ for the absolute magnitude of the turnover, which is consistent with previous studies (e.g., Fleming et al. 1995). Since the dispersion of the Gaussian function has been shown to have only a narrow range of values centered on $\sigma_{gauss} = 1.4$ (Harris 1991; Jacoby et al. 1992), we have decided to adopt this value. A non-linear weighted least-squares fit of the GCLF of HCG 22a, using $M_V = -7.4 \pm 0.2$, $\sigma_{gauss} = 1.4$ and a distance of 54.1 Mpc, gives $A = 38.4 \pm 8.1$ with $\chi^2_\nu = 1.4$. For HCG 90c, we found $A = 51.3 \pm 7.6$ and $\chi^2_\nu = 1.9$, using a distance of 53.9 Mpc. Figure 8 and 9 show the GCLF, with the best-fit Gaussian function, for HCG 22a and HCG 90c, respectively. Counts of stellar-like objects in the galaxy and control fields are given in Table 2 and 3 for HCG 22a and HCG 90c, respectively.

3.2. Radial Distribution

In addition to correcting globular cluster counts for incomplete sampling of the GCLF as discussed above, it is also necessary to correct the counts for the limited areal coverage around each galaxy.

The globular cluster radial distribution was measured by dividing the galaxy images into several annuli centered on each galaxy. For each annulus, the total number of globular cluster candi-

dates were corrected for incompleteness and subtracted by the properly normalized control field counts.

The radial distribution was characterized using a power-law of the form, $\sigma = AR^{\alpha}$ (e.g., Fleming et al. 1995). Using weighted non-linear least-squares, the best-fit values for the radial distribution of HCG 22a was determined to be $A = 7.2 \pm 1.28$ and $\alpha = -2.01 \pm 0.30$, with $\chi^2_\nu = 1.3$. Figure 10 depicts the radial distribution of globular cluster candidates for HCG 22a along with the best-fit power-law.

For HCG 90c, the best-fit values for the radial distribution was found to be $A = 13.99 \pm 1.42$ and $\alpha = -1.20 \pm 0.16$, with $\chi^2_\nu = 1.5$. Figure 11 depicts the radial profile of the globular cluster candidates, along with the best-fit power-law.

A useful comparison can be made between the spatial extent of the globular cluster system and the stellar halo of the parent galaxy. Figure 12 shows the comparison of the radial profile of the globular cluster system and the surface brightness for HCG 22a. The surface brightness data has been taken from Franx et al. (1989) and has been scaled vertically to match the GC profile near its center. A fit to the radial dependence of the halo surface brightness, μ, gives, $\mu \sim R^{-2.3}$, which is consistent with the slope of the radial profile of the GCs ($\alpha = -2.01 \pm 0.3$). Thus, the globular cluster system is as spatially extended as the halo light of HCG 22a, which is consistent with other studies where the GC profiles are either similar to or more extended than the galaxy halo (e.g., Fleming et al. 1995).

The surface brightness profile of HCG 90c was determined from Penereiro (1994) and is compared with the radial distribution of its globular cluster population in Figure 13. The surface brightness profile has been scaled vertically to match the globular cluster distribution. A fit to the halo profile gives a slope of $\mu \sim R^{-1.5}$ and hence, the globular cluster population is spatially more extended than the galaxy halo. We also note that the halo light of HCG 90c is not well defined due to the high surface brightness of the intra-group light (White et al. 2001).

3.3. Specific Frequency

As mentioned in Section 1, a useful way of quantifying the globular cluster population of different galaxies is to compare values of specific frequency, $S_N = N_{tot} 10^{0.4(M_V+15)}$. The first step in calculating S_N is to determine the total number of globular clusters, N_{tot}. The power-law radial distribution function, $\sigma = AR^{\alpha}$, must be integrated from an inner to an outer radius in order to account for the globular clusters that were missed due to spatial incompleteness. Also, the number of globular clusters must be corrected for incomplete coverage of the luminosity function.

3.3.1. Hickson Compact Group 22a

In order to integrate the power-law radial distribution function, inner and outer radial limits must be chosen. Globular cluster distributions normally do not extend to radii inward of 1 kpc from the center of the parent galaxy (e.g., Harris 1991; Bridges, Hanes, & Harris 1991), the most likely cause being tidal shocking and dynamical friction which have destroyed globular clusters at distances close to the galaxy center (e.g., Weinberg 1993). For an outer radius, globular cluster systems generally do not extend past 50 kpc from the center of a typical elliptical galaxy (e.g., Harris & van den Bergh 1981; Hanes & Harris 1986; Fleming et al. 1995). Thus for this study, an inner radius of 1 kpc and an outer radius of 50 kpc was adopted for HCG 22a and 90c. These radial limits for HCG 22a correspond to angular distances of $0.06'$ and $3.1'$. A consistency check is provided by the fact that the radial counts for HCG 22a and 90c appear to reach background levels approximately 50 kpc from the galaxy center.

The integral of the power-law density profile gives $N_{tot} = \int \sigma_{cl}\, 2\pi R\; dR$, where σ_{cl} represents the number density of globular clusters. For HCG 22a we have $N_{tot} = 2\pi A \int_{0.06'}^{3.18'} R^{\alpha+1} dR$. Solving this equation gives the total number of globular clusters, $N_{tot} = 179 \pm 54$ *before* including the correction for faint globular clusters that are below our detection limit. If the outer radius was set to a smaller value, say 25 kpc, the total number of globular clusters would be ~ 148 and hence, N_{tot} is not extremely sensitive to our chosen value of an outer radius for a steep radial slope of $\alpha \sim -2.0$.

After correcting for the radial incompleteness of

detected globular clusters, the incomplete coverage of the luminosity function must be accounted for. Since the luminosity function was assumed to be a Gaussian, the area under the Gaussian function that was accounted for will give a measure of the percentage of observed globular clusters. Integrating the curve from $-\infty$ to the photometric limit of the data ($V = 24.6$), indicates that $11\pm3\%$ of the distribution was observed. Correcting N_{tot} for the unobserved part of the luminosity function gives $N_{tot}^{cor} = 1590 \pm 854$.

Once the total number of globular clusters was determined, the specific frequency was calculated from the absolute V magnitude of the parent galaxy. Using an absolute magnitude of $M_V = -22.31 \pm 0.07$ as given by NED[3], the specific frequency was determined to be $S_N = 1.9 \pm 1.0$ for HCG 22a (using $H_0 = 75$ km s^{-1}Mpc^{-1}, we find $S_N = 1.7 \pm 0.6$).

3.3.2. Hickson Compact Group 90c

The specific frequency for HCG 90c was calculated in the analogous way as for HCG 22a. The total number of globular clusters, for the chosen radial limits of 1 kpc to 50 kpc ($0.07'$ to $3.5'$), was determined to be $N_{tot} = 270 \pm 28$. Changing the outer radius to 25 kpc yields $N_{tot} \sim 150$ and thus the total number of globular clusters is sensitive to the choice of an outer radius because of the shallow radial profile with $\alpha \sim -1.2$.

Correcting for the unobserved part of the luminosity function, we determined that $13 \pm 3\%$ of the total number of globular clusters were observed and that $N_{tot}^{cor} = 2136 \pm 718$. Using an absolute magnitude of $M_V = -21.99 \pm 0.03$, we find that $S_N = 3.4 \pm 1.1$ for HCG 90c (using $H_0 = 75$ km s^{-1}Mpc^{-1}, we find $S_N = 4.4 \pm 1.3$).

4. Discussion

In this paper we have investigated the globular cluster population of two prominent elliptical galaxies, each located near the center of a Hickson compact group. The globular cluster population has been characterized by measuring the number of globular clusters per unit galaxy luminosity (S_N), radial distributions, and the globular cluster luminosity function. Although our sample is limited to only two compact group galaxies, we can draw some tentative conclusions.

The most important aspect of this study is the determination of the specific frequency of HCG 22a and HCG 90c. As mentioned in section 1, specific frequency values for field ellipticals generally range from $S_N = 2 - 3$, in contrast to values measured for cD galaxies at the center of rich clusters ($S_N = 10-20$). Although S_N seems to follow a general trend that as the local density increases the number of globular clusters per unit galaxy luminosity also increases, there are exceptions (e.g., Harris, Pritchet, & McClure 1995; Woodworth & Harris 2000). The evidence seems to suggest that a high density environment, at least at the current epoch, may be a necessary but not a sufficient condition for the formation of high S_N galaxies. The relatively low values of S_N for HCG 22a and 90c ($S_N = 1.9 \pm 1.0$ and $S_N = 3.4 \pm 1.1$, respectively) suggests that these galaxies formed their globular clusters at a time when they were located in a "field-like" low density environment.

The exact nature of Hickson compact groups has been controversial since some studies have suggested that the majority of compact groups are chance projections of large filamentary structures (Hernquist, Katz, & Weinberg 1995) or a superposition of galaxies in a much larger group or poor cluster (Walke & Mamon 1989). N-body simulations have indicated that, given the small crossing times and low velocity dispersions (Hickson et al. 1992), group member galaxies would combine to form a single elliptical galaxy on the order of a few crossing times (e.g., Barnes 1985; Mamon 1987; but see Mamon 2000) and several examples of isolated ellipticals which may be the surviving remnants of galaxy groups have been discovered (Mulchaey & Zabludoff 1999). This suggests that if compact groups are gravitationally bound, group members may be just beginning to come together at the present epoch and that during the time of globular cluster formation, these galaxies were situated in a lower density environment. This scenario is consistent with the specific frequency values measured for HCG 22a and 90c.

Evidence to support the hypothesis that these groups are bound structures include; the detection of H_I and X-rays (Williams & Rood 1987;

[3]The NASA/IPAC Extragalactic Database (NED) is operated by the Jet Propulsion Laboratory, California Institute of Technology, under contract with the National Aeronautics and Space Administration.

Pildis, Bregman, & Evrard 1995; Ponman et al. 1996), indicating significant dynamical evolution and galaxy interaction, the decrease in the relative number of spirals with decreasing group crossing times (Hickson et al. 1992), and the presence of tidal tails and debris in some compact groups (Hunsberger, Charlton, & Zaritsky 1996).

As mentioned in section 1, both HCG 22 and 90 are weak X-ray emitters. Radial velocity measurements imply that both HCG 22a and 90c are located near the bottom of their group potential well. Also, HCG 90b is clearly interacting with HCG 90d (Plana et al. 1999). HCG 90 has also been shown to contain a spatially extended, diffuse, light component (White et al. 2001). These facts suggests that both HCG 22 and 90 are gravitationally bound structures.

In recent years, it has been shown that the globular cluster systems of many large elliptical galaxies contain two or more chemically distinct subpopulations, usually inferred on the basis of color information (e.g., Ostrov, Geisler, & Forte 1993; Geisler, Lee, & Kim 1996; Côte et al. 1998). A number of different theories have been proposed to explain the origin of these different globular cluster populations; among these are models in which two or more bursts of globular cluster formation occur (e.g., Ashman & Zepf 1992; Forbes & Forte 2000) or accretion of globular clusters from other galaxies (e.g., Côte et al. 1998, 2000). Given the rather unique environments represented by compact groups, and the roles that mergers may have played, it would be interesting to ascertain whether Hickson compact group galaxies also exhibit multiple globular cluster populations. Unfortunately, the V-R information provided by this investigation does not give us a sufficiently long color baseline to explore this possibility.

5. Conclusions

We have studied the globular cluster systems around the early-type galaxies HCG 22a (NGC 1199) and 90c (NGC 7173) using V and R band data obtained from ESO's NTT. Globular clusters have been detected as a statistical excess of star-like objects surrounding each galaxy. Object detection and classification was performed using FOCAS on galaxy-subtracted images.

The specific frequency of each galaxy was measured assuming a turnover and dispersion of the globular cluster luminosity function. We found that for HCG 22a, $S_N = 1.9 \pm 1.0$, and for HCG 90c, $S_N = 3.4 \pm 1.1$. The total number of globular clusters for HCG 22a was determined to be $N_{tot} = 1590 \pm 854$ and for HCG 90c we found $N_{tot} = 2136 \pm 718$. We also derived the globular cluster surface density profiles and found that for HCG 22a, the underlying starlight is as extended as the GC system. For HCG 90c, we found that the GC system is more extended than the galaxy halo.

From the results of this study, it is clear that further observations are needed to help understand the formation of globular clusters and the nature of Hickson compact groups. Observations which clearly reach the turnover in the globular cluster luminosity function would be of great value since they would provide a more robust determination of the GCLF, radial distribution, and specific frequency. Observations design to detect any bimodality in the color distribution would provide invaluable information on the past history of the globular cluster systems.

Additional observations of a larger sample of compact group galaxies would allow the investigation of potential correlations between galaxy luminosity and S_N (since the local environment would be the same for a pair of galaxies in the same group) or other factors such as X-ray luminosity, mass-to-light ratio, and distance from the group dynamical center.

The authors would like to thank the referee for useful comments and suggestions. This research has made use of the NASA/IPAC Extragalactic Database (NED) which is operated by the Jet Propulsion Laboratory, California Institute of Technology, under contract with the National Aeronautics and Space Administration. WAB is grateful for the support of the Reinhardt and Sumner fellowships. MJW acknowledges support from NSF grant AST 00-71149 and from NSERC of Canada.

REFERENCES

Ashman, K. M., & Zepf, S. E. 1992, ApJ, 384, 50

Barnes, J. 1985, MNRAS, 215, 517

Blakeslee, J. P. 1999, AJ, 118, 1506

Bridges, T. J., Hanes, D. A., & Harris, W. E. 1991, AJ, 101, 469

Burstein, D. & Heiles, C. 1982, AJ, 87, 1165

Côté, P., Marzke, R. O., & West, M. J. 1998, AJ, 501, 554

Côté, P., Marzke, R. O., West, M. J. & Minniti, D. 2000, ApJ, 533, 869

Fleming, D. E. B., Harris, W. E., Pritchet, C. J., & Hanes, D. A. 1995, AJ, 109, 1044

Forbes, D.A., Brodie, J.P. & Grillmair, C.J. 1997, AJ, 113, 1652

Forbes, D.A., & Forte, J. C. 2000, MNRAS, 322, 257

Franx, M., Illingworth, G., & Heckman, T. 1989, AJ, 98, 538

Gebhardt, K. & Kissler-Patig, M. 1999, AJ, 118, 1526

Geisler, D., Lee, M. G., & Kim, E. 1996, AJ, 111, 1529

Hanes, D. A., & Harris, W. E. 1986, ApJ, 309, 564

Harris, W. E. 1990, PASP, 102, 949

Harris, W. E. 1991, ARA&A, 29, 543

Harris, W. E., Pritchet, C. J., & McClure, R. D. 1995, ApJ, 441, 120

Harris, W. E., & van den Bergh, S. 1981, AJ, 86, 1627

Hernquist, L., Katz, N. S., & Weinberg, D. H. 1995, ApJ, 442, 57

Hickson, P. 1982, ApJ, 255, 382

Hickson, P. 1994, Atlas of Compact Groups of Galaxies (Switzerland: Gordon and Breach Science Publishers)

Hickson, P., Mendes de Oliveira, C., Huchra, J. P., & Palumbo, G. G. C. 1992, ApJ, 399, 353

Hunsberger, S. D., Charlton, J. C., & Zaritsky, D. 1996, ApJ, 462, 50

Jacoby, G. H., Branch, D., Ciardullo, R., Davies, R. L., Harris, W. E., Pierce, M. J., Pritchet, C. J., Tonry, J. L., & Welch, D. L. 1992, PASP, 104, 599

Jarvis, J. F., & Tyson, J. F. 1981, AJ, 86, 476

Kissler-Patig, M. 2000, Reviews In Modern Astronomy, 13, 13

Kundu, A., & Whitmore, B.C. 2001, AJ, 121, 2950

Landolt, A. U. 1992, AJ, 104, 340

Longo, G., Busarello, G., Lorenz, H., Richter, G., & Zaggia, S. 1994, A&A, 282, 418

Mamon, G. A. 1987, ApJ, 321, 622

Mamon, G. A. 2000, in ASP Conf. Ser. 209, Small Galaxy Groups, ed. M. Valtonen & C. Flynn (San Fransico: ASP), 217

Mulchaey, J. S. & Zabludoff, A. I. 1999, ApJ, 514, 133

Ostrov, P., Geisler, D., & Forte, J. C. 1993, ApJ, 105, 1762

Penereiro, J. C., de Carvalho, R. R., Djorgovski, S., & Thompson, D. 1994, A&AS, 108, 461

Peterson, C. 1993, in ASP Conf. Ser. 50, Structure and Dynamics of Globular Clusters, ed. S.G. Djorgovski & G. Meylan (San Fransico: ASP), 337

Pildis, R. A., Bregman, J. N., & Evrard, A. E. 1995, ApJ, 443, 514

Plana, H., Mendes de Oliveira, C., Amram, P., & Boulesteix, J. 1999, AJ, 116, 2123

Ponman, T. J., Bourner, P. D. J., Ebeling, H., & Böhringer, H. 1996, MNRAS, 283, 690

Ratnatunga, K. U., & Bahcall, J. N. 1985, ApJS, 59, 63

Schweizer, F. 1986, in Nearly Normal Galaxies, ed. S. Faber (New York: Springer), 18

Secker, J. 1995, PASP, 107,496

Walke, D. G., & Mamon, G. A. 1989, A&A, 295, 291

Weinberg, M. D. 1993, in ASP Conf. Ser. 43, The Globular Cluster-Galaxy Connection, ed. G.E. Smith & J.P. Brodie (San Fransico: ASP), 689

West, M.J. 1994, MNRAS, 265, 755

Williams, B. A., & Rood, H. J. 1987, ApJS, 63, 265

White, P., Bothun, G., Barkhouse, W.A. & West, M.J. 2001, in preparation

Woodworth, S. C., & Harris, W. E. 2000, AJ, 119, 2699

Valdes, F. 1993, FOCAS User's Guide, NOAO document

Fig. 1.— V band image of Hickson compact group 22a (NGC 1199).

Fig. 2.— V band image of Hickson compact group 90 with HCG 90c located near the center position.

Fig. 3.— Positions of globular cluster candidates surrounding HCG 22a with $V \leq 24.6$. The central 70 pixel masked-out region is shown along with the galaxy center at $X = 885$ and $Y = 647$ pixels. Only objects having radii $70 \leq R \leq 441$ pixels are shown. Note the concentration of star-like objects around the center of HCG 22a.

Fig. 4.— Positions of globular cluster candidates surrounding HCG 90c with $V \leq 24.6$. The central 60 pixel masked-out region is shown along with the galaxy center at $X = 887$ and $Y = 652$ pixels. Only those objects having radii $60 \leq R \leq 535$ pixels are shown, excluding the area in the lower left quadrant which was masked out due to the presence of HCG 90b and d. Note the concentration of star-like objects around the center of HCG 90c.

Fig. 5.— Color-magnitude diagram of the globular cluster candidates surrounding HCG 22a. Note the enhanced concentration of stellar-like objects near $V - R = 0.6$.

Fig. 6.— Color-magnitude diagram of the globular cluster candidates surrounding HCG 90c. Note the enhanced concentration of stellar-like objects near $V - R = 0.5$.

Fig. 7.— Color-magnitude diagram of stellar-like objects in the control field. Note that objects appear to be scattered to a greater extent than those found for HCG 22a and 90c.

Fig. 8.— Globular cluster luminosity function of HCG 22a. The best-fit Gaussian function is shown as the dashed line with a turnover of $m_V = 26.3 \pm 0.2$ and a dispersion of $\sigma = 1.4$.

Fig. 9.— Globular cluster luminosity function of HCG 90c. The best-fit Gaussian function is shown as the dashed line with a turnover of $m_V = 26.0 \pm 0.2$ and a dispersion of $\sigma = 1.4$.

Fig. 10.— Radial distribution of globular clusters around HCG 22a. The best-fit power-law function, $\sigma \sim R^{-2.01 \pm 0.30}$, is shown as the dashed line. The radius is given as the geometric mean of the individual annulii,$< R >= \sqrt{R_{in} R_{out}}$, and σ is the number of star-like objects per arcminute^2.

Fig. 11.— Radial profile of globular clusters surrounding HCG 90c. The best-fit power-law, $\sigma \sim R^{-1.20 \pm 0.16}$ is shown as a dashed line. The radius and σ are as defined for HCG 22a.

Fig. 12.— The radial profile of the globular cluster system of HCG 22a (dashed line) compared to the R-band galaxy surface brightness from Franx et al. (1989) (solid line). The surface brightness profile has been scaled vertically in order to match the GC profile near the center. From the figure, it is clear that the globular cluster system is as spatially extended as the halo light of the parent galaxy. The slope of the power-law fit to the GC profile is $\alpha = -2.01 \pm 0.3$ and for the halo light the slope is $\alpha \sim -2.3$.

Fig. 13.— The radial profile of the globular cluster system of HCG 90c (solid line) compared to the R-band galaxy surface brightness from Penereiro (1994) (dashed line). The surface brightness profile has been scaled vertically in order to match the GC profile near the center. From the figure, it is clear that the globular cluster system is more spatially extended than the halo light of the parent galaxy. The slope of the power-law fit to the GC profile is $\alpha = -1.20 \pm 0.16$ and for the halo light the slope is $\alpha \sim -1.5$.

TABLE 1
GENERAL PROPERTIES OF HCG 22A AND HCG 90C

	HCG 22a[1]	HCG 90c
α (1950)	03 01 18.2	21 59 08.8
δ (1950)	-15 48 30	-32 12 58
l (deg)	199.22	14.98
b (deg)	-57.31	-53.08
Hubble Type	E2	E0
V_o (km s^{-1})	2705	2696
B_T(mag)	12.24	12.73
B-R (mag)	1.62	2.23

[1]Table information from Hickson (1994).

Table 2
Globular Cluster Counts: HCG 22a

V	$N_{gal.}$	N_{bkg}	N
22.1	3.0 ± 1.7	0.6 ± 0.4	2.4 ± 1.8
22.3	3.0 ± 1.7	2.2 ± 0.8	0.8 ± 1.9
22.5	0.0 ± 0.0	0.8 ± 0.5	-0.8 ± 0.5
22.7	5.0 ± 2.2	1.4 ± 0.6	3.6 ± 2.3
22.9	7.0 ± 2.6	2.8 ± 0.9	4.2 ± 2.8
23.1	3.1 ± 1.8	0.6 ± 0.4	2.5 ± 1.8
23.3	9.3 ± 3.1	1.6 ± 0.3	7.6 ± 3.1
23.5	8.1 ± 2.9	2.8 ± 0.9	5.4 ± 3.0
23.7	14.2 ± 4.2	4.4 ± 1.1	9.7 ± 4.3
23.9	16.1 ± 4.4	7.2 ± 1.4	9.0 ± 4.6
24.1	10.6 ± 3.4	10.0 ± 1.6	0.6 ± 3.8
24.3	35.4 ± 6.6	8.8 ± 1.7	26.6 ± 6.8
24.5	30.2 ± 7.0	12.0 ± 2.0	18.2 ± 7.3

Note.—Column 1 gives the mid-bin V magnitude. Columns 2 and 3 gives the raw counts of stellar-like objects in the galaxy and control field. Column 4 gives the background-corrected counts of stellar-like objects in the galaxy field.

Table 3
Globular Cluster Counts: HCG 90c

V	$N_{gal.}$	N_{bkg}	N
22.1	6.0 ± 2.4	0.6 ± 0.4	5.4 ± 2.5
22.3	6.0 ± 2.4	2.5 ± 0.9	3.5 ± 2.6
22.5	8.0 ± 2.8	0.9 ± 0.5	7.1 ± 2.9
22.7	6.0 ± 2.4	1.6 ± 0.4	4.4 ± 2.5
22.9	13.0 ± 3.6	3.1 ± 1.0	9.9 ± 3.7
23.1	15.0 ± 3.9	0.6 ± 0.4	14.4 ± 3.9
23.3	6.0 ± 2.4	1.9 ± 0.8	4.1 ± 2.6
23.5	10.0 ± 3.2	3.1 ± 1.0	6.9 ± 3.3
23.7	20.0 ± 4.5	5.0 ± 1.2	15.0 ± 4.6
23.9	22.0 ± 4.7	8.1 ± 1.6	13.9 ± 5.0
24.1	26.0 ± 5.1	11.2 ± 1.9	14.8 ± 5.4
24.3	50.1 ± 7.4	9.9 ± 1.9	40.2 ± 7.7
24.5	38.8 ± 6.9	13.5 ± 2.3	25.4 ± 7.2

Note.—Column 1 gives the mid-bin V magnitude. Columns 2 and 3 gives the raw counts of stellar-like objects in the galaxy and control field. Column 4 gives the background-corrected counts of stellar-like objects in the galaxy field.

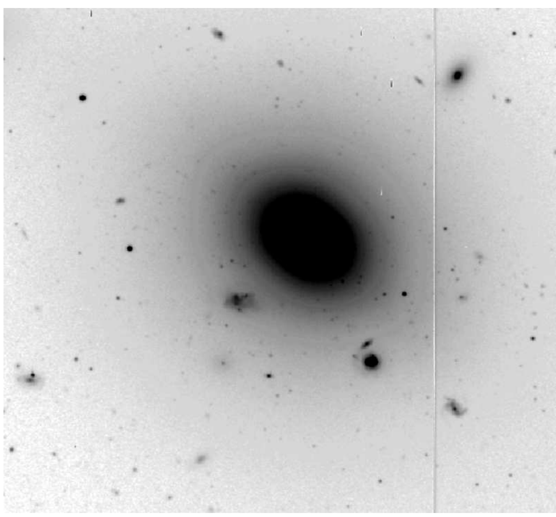

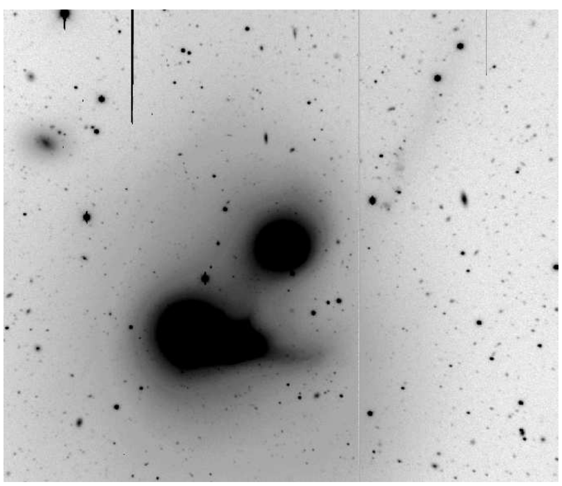

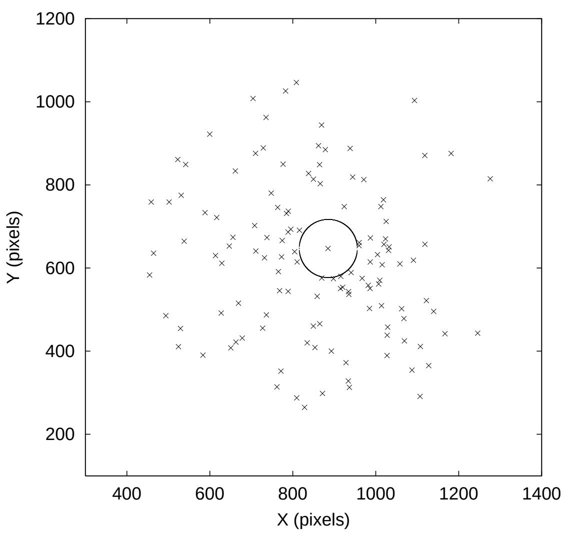
1200
1000
800
600
400
200
Y (pixels)
400
600
800
1000
1200
1400
X (pixels)

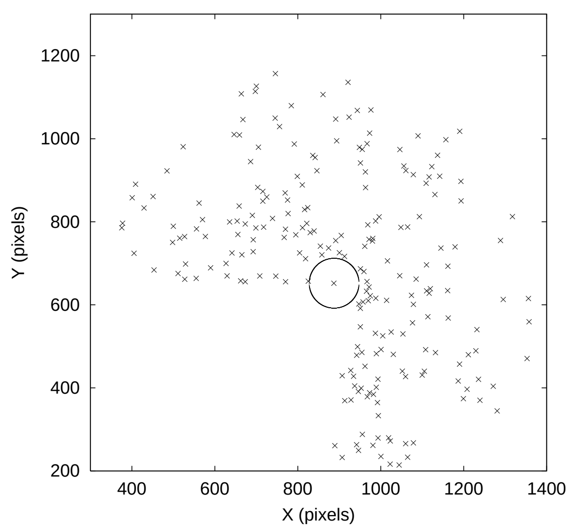
1200
1000
800
600
400
200
400
600
800
1000
1200
1400
Y (pixels)
X (pixels)

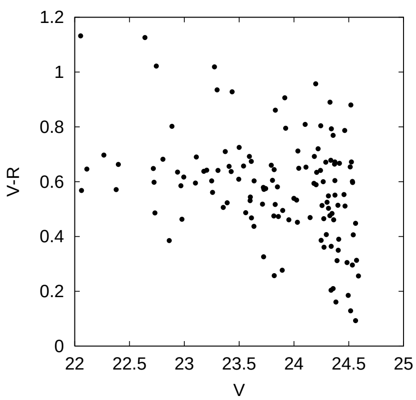

1.2
1
0.8
0.6
0.4
0.2
0
V-R
22
22.5
23
23.5
24
24.5
25
V

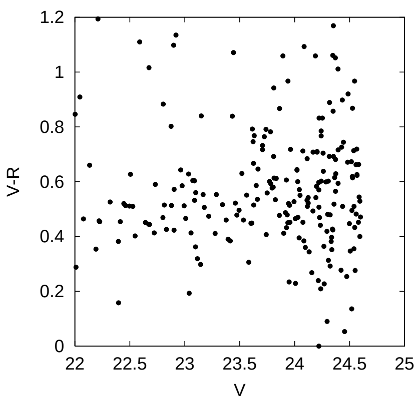

1.2
1
0.8
0.6
0.4
0.2
0
V-R
22
22.5
23
23.5
24
24.5
25
V

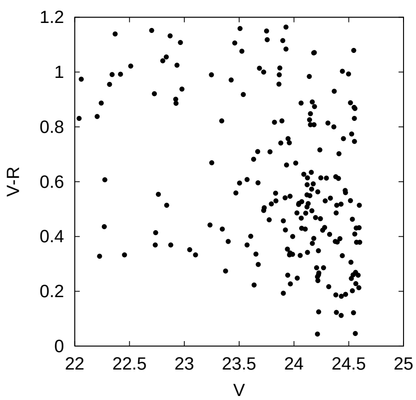

1.2
1
0.8
0.6
0.4
0.2
0
V-R
22
22.5
23
23.5
24
24.5
25
V

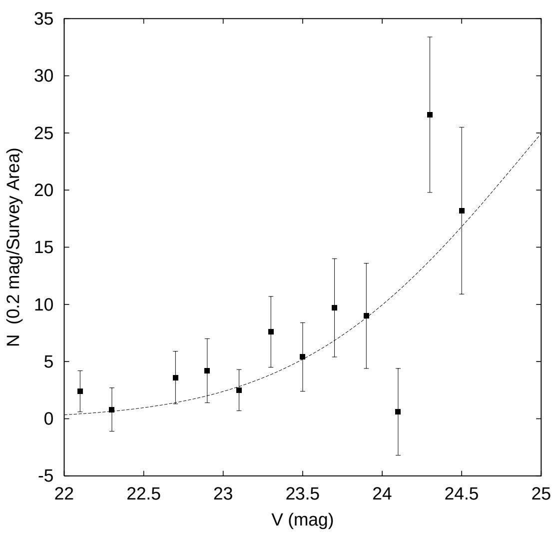
35
30
25
20
15
10
5
0
-5
N (0.2 mag/Survey Area)
22
22.5
23
23.5
24
24.5
25
V (mag)

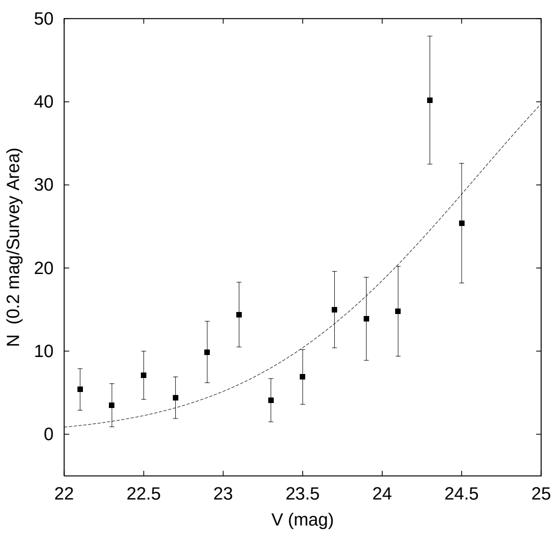

N (0.2 mag/Survey Area)
V (mag)
50
40
30
20
10
0
22
22.5
23
23.5
24
24.5
25

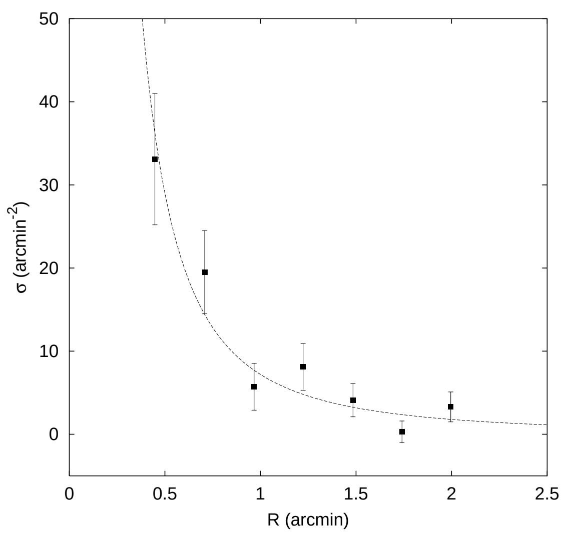

50
40
30
20
10
0
σ (arcmin^{-2})
0
0.5
1
1.5
2
2.5
R (arcmin)

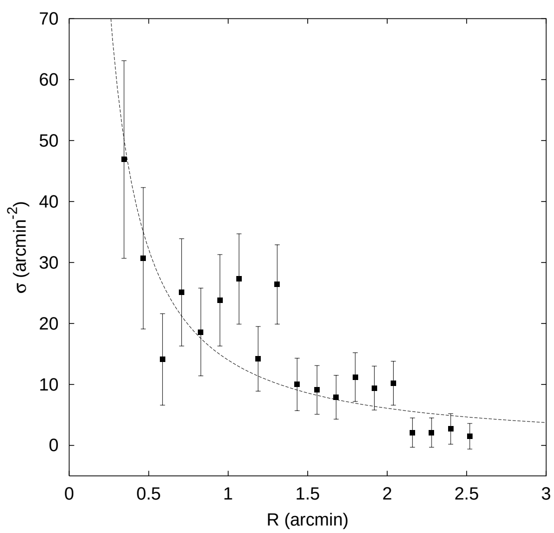
σ (arcmin^-2)
70
60
50
40
30
20
10
0
0
0.5
1
1.5
2
2.5
3
R (arcmin)

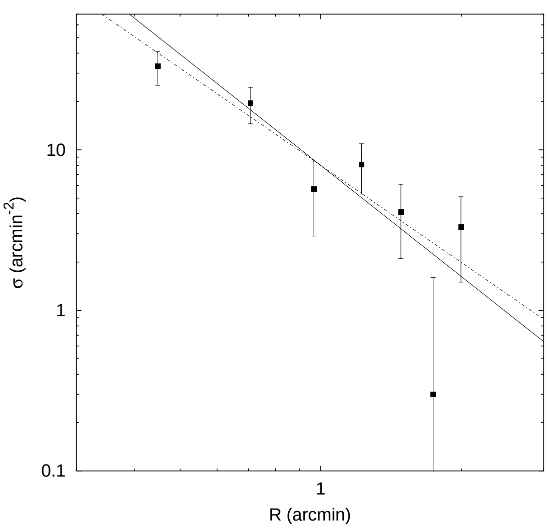
10
1
0.1
σ (arcmin^{-2})
1
R (arcmin)

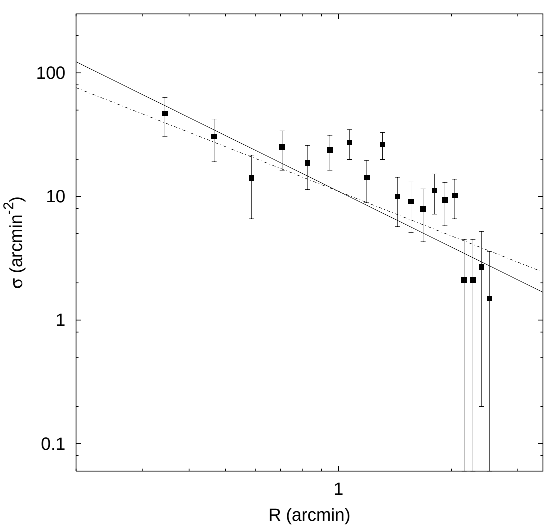
100
10
1
0.1
σ (arcmin-2)
1
R (arcmin)